AIAA Aviation
16-20 June 2014, Atlanta, GA
32nd AIAA Applied Aerodynamics Conference

Co-Flow Jet Airfoil Trade Study Part I : Energy Consumption and Aerodynamic Efficiency

Alexis Lefebvre *, G.-C. Zha †
Dept. of Mechanical and Aerospace Engineering
University of Miami
Coral Gables, Florida 33124
E-mail: gzha@miami.edu

Abstract

This paper is the Part I of a parametric study on CFJ airfoils. A trade study is performed for a series of CFJ airfoils based on the NACA 23121 airfoil on the injection location, suction location, suction size, angle of attack (AoA), momuntum coefficient , airfoil thickness, Reynolds number and their resulting effects on the lift, drag, moment and energy consumption. The two dimensional flow is simulated using steady and unsteady Reynolds Average Navier-Stokes (RANS). A 5th order WENO scheme for the inviscid flux, a 4th order central differencing model for the viscous terms and the one equation Spalart-Allmaras turbulence model are used. The Mach number is 0.15 and Reynolds number is 6.4×10^6. CFJ airfoils are shown to be effective at increasing the lift and reducing the drag drastically. The jet location and the AoA are found to be influential parameters for the energy consumption and aerodynamic efficiency. The pitch-down moment and energy consumption are reduced when the suction is located more upstream. The lift and drag are improved when the suction is located more downstream. The pumping power decreases when the AoA is increased before the apparition of a recirculation region. When the AoA is further increased, the energy consumption is increased because of the increased jet total pressure losses due to the strong adverse pressure gradient and separated flow.

* Graduate Student
† Professor, AIAA Associate Fellow

Nomenclature

CFJ	Co-flow jet
AoA	Angle of attack
LE	Leading Edge
TE	Trailing Edge
S	Planform area
c	Profile chord
U	Flow velocity
q	Dynamic pressure $0.5\,\rho\,U^2$
p	Static pressure
ρ	Air density
$\dot{m}$	Mass flow
M	Mach number
ω	Pitching Moment
P	Pumping power
∞	Free stream conditions
$_j$	Jet conditions
C_L	Lift coefficient $L/(q_\infty\,S)$
C_D	Drag coefficient $D/(q_\infty\,S)$
C_M	Moment coefficient $\omega/(q_\infty\,S\,c)$
C_p	Pressure coefficient $(p-p_\infty)/q_\infty$
C_μ	Jet momentum coef. $\dot{m}_j\,U_j/(q_\infty\,S)$
E	Corrected aerodynamic efficiency $L/(D+P/V_\infty)$
Pc	Power coefficient $L/(q_\infty\,S\,V_\infty)$

1 Introduction

A high performance airfoil should have a combination of high maximum lift, high cruise L/D and relatively low nose-down moment for stability. To enhance the maximum lift the use of flaps and slats are often necessary. The NACA 23021 airfoil with two different flap configurations have been experimentally studied by T. A. Harris in [1]. The maximum C_L achieved by the slotted flapped airfoil with a large flap deflection is 2.49. However the very high C_D of 0.17 and C_M of -0.37 render this performance point unusable in practice. A more reasonable flap deflection angle achieved a maximum C_L of 2.0 with an associated C_D of 0.045 and C_M of -0.39 for the best configuration. The flapped configuration suffers from an important drag and nose-down moment that reduces the airfoil aerodynamic efficiency and requires important tail force to balance, further reducing the airplane efficiency. In addition, those devices introduce a significant weight penalty and complexity in the wing structure.

Recently, a zero-net mass-flux(ZNMF) co-flow jet (CFJ) flow control airfoil developed by Zha et al. [2, 3, 4, 5, 6, 7, 8, 9, 10] based on fluidic actuators is demonstrated to achieve radical lift augmentation, stall margin increase, drag reduction and moderate nose-down moment for stationary and pitching airfoils. In the CFJ airfoil concept an injection slot near the leading edge (LE) and a suction slot near the trailing edge (TE) on the airfoil suction surface are created as sketched in Fig. 1. A small mass flow is withdrawn into the airfoil near the TE, pressurized and energized by a pumping system inside the airfoil, and then injected near the LE tangentially to the main flow. The whole process does not add any mass flow to the system and hence is a ZNMF flow control. The energy expenditure is low [3, 8, 9] and the implementation is straightforward.

In a previous study [11] the effect of injection slot size on the lift and drag was investigated on a NACA0025

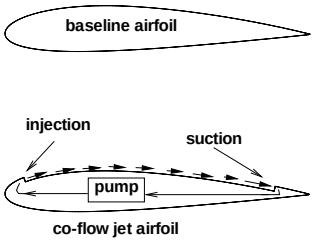

Figure 1: CFJ airfoil concept

CFJ airfoil. However, no efforts have been made to systematically study the power consumption or the moment of the CFJ airfoil, which are crucial data for the airfoil design. This paper conduct a trade study for a series of CFJ airfoils based on the NACA 23121 airfoil on the injection location, suction location, suction size, angle of attack (AoA), momuntum coefficient , airfoil thickness, Reynolds number and their resulting effects on the lift, drag, moment and energy consumption. The baseline airfoil NACA 23121 is chosen for its small nose-up moment, which is intended to achieve low moment CFJ airfoils.

2 CFJ Parameters

This section will introduce the definitions of several parameters that are important for CFJ airfoil performance.

2.1 Lift and Drag Calculation

The momentum and pressure at the injection and suction slots produce a reactionary force, which is automatically measured by the force balance in wind tunnel testing. However, for CFD simulation, the full reactionary force needs to be included. Using control volume analysis, the reactionary force can be calculated using the flow parameters at the injection and suction slot opening surfaces. Zha et al. [3] give the following formulations to calculate the lift and drag due to the jet reactionary force for a CFD simulation. By considering the effects of injection and suction jets on the CFJ airfoil, the expressions for these reactionary forces are given as :

$$F_{x_{cfj}} = (\dot{m}_j V_{j1} + p_{j1} A_{j1}) * cos(\theta_1 - \alpha) - (\dot{m}_j V_{j2} + p_{j2} A_{j2}) * cos(\theta_2 + \alpha) \tag{1}$$

$$F_{y_{cfj}} = (\dot{m}_{j1} V_{j1} + p_{j1} A_{j1}) * sin(\theta_1 - \alpha) + (\dot{m}_{j2} V_{j2} + p_{j2} A_{j2}) * sin(\theta_2 + \alpha) \tag{2}$$

where the subscripts 1 and 2 stand for the injection and suction respectively, and θ_1 and θ_2 are the angles between the injection and suction slot's surface and a line normal to the airfoil chord. α is the angle of attack.

The total lift and drag on the airfoil can then be expressed as:

$$D = R'_x - F_{x_{cfj}} \tag{3}$$

$$L = R'_y - F_{y_{cfj}} \tag{4}$$

where R'_x and R'_y are the surface integral of pressure and shear stress in x (drag) and y (lift) direction excluding the internal ducts of injection and suction. For the CFD simulation, the total lift and drag are calculated using Eqs.(3) and (4).

2.2 Jet Momentum Coefficient

The jet momentum coefficient C_μ is a parameter used to quantify the jet intensity. It is defined as :

$$C_\mu = \frac{\dot{m}V_j}{\frac{1}{2}\rho_\infty {V_\infty}^2 S} \tag{5}$$

where $\dot{m}$ is the injection mass flow, V_j the injection velocity, ρ_∞ and V_∞ denote the free stream density and velocity, and S is the planform area.

2.3 Power Coefficient

The CFJ can be implemented by mounting a pumping system inside the wing that withdraws air from the suction slot and blows it into the injection slot. The power consumption can be determined by the jet mass flow and total enthalpy change as the following :

$$P = \dot{m}(H_{t1} - H_{t2}) \tag{6}$$

where H_{t1} and H_{t2} are the total enthalpy in the injection cavity and suction cavity respectively, P is the Power required by the pump and $\dot{m}$ the jet mass flow rate. Introducing the pump efficiency η and total pressure ratio of the pump $\Gamma = \frac{P_{t1}}{P_{t2}}$, the power consumption can be expressed as :

$$P = \frac{\dot{m}C_p T_{t2}}{\eta}(\Gamma^{\frac{\gamma-1}{\gamma}} - 1) \tag{7}$$

The power consumption can be expressed as a power coefficient below:

$$P_c = \frac{P}{\frac{1}{2}\rho_\infty V_\infty^3 S} \tag{8}$$

2.4 Corrected Aerodynamic Efficiency

The conventional airfoil aerodynamic efficiency is defined as :

$$\frac{L}{D} \tag{9}$$

For the CFJ airfoil, this ratio still represents the aerodynamic efficiency in the sense of pure aerodynamic forces. However since CFJ active flow control consumes energy, the CFJ corrected aerodynamic efficiency is modified to take into account the energy consumption of the pump. The formulation of the corrected aerodynamic efficiency for CFJ airfoils is :

$$(\frac{L}{D})_c = \frac{L}{D + \frac{P}{V_\infty}} \tag{10}$$

where V_∞ is the free stream velocity, P is the pumping power, and L and D are the lift and drag generated by the CFJ airfoil. This formulation converts the power consumed by the CFJ into the drag of the airfoil. If the pumping power is set to 0, this formulation returns to the formulation of a conventional airfoil.

3 CFD Simulation Setup

3.1 CFD Code

The FASIP (Flow-Acoustics-Structure Interaction Package) CFD code is used to conduct the numerical simulation. The 2D Reynolds averaged Navier-Stokes (RANS) equations with one-equation Spalart-Allmaras [12] turbulence model is used. A 5th order WENO scheme for the inviscid flux [13, 14, 15, 16, 17, 18] and a 4th order central differencing for the viscous terms [13, 17] are employed to discretize the Navier-Stokes equations. The low diffusion E-CUSP scheme used as the approximate Riemann solver suggested by Zha et al [14] is utilized with the WENO scheme to evaluate the inviscid fluxes. Implicit time marching method using Gauss-Seidel line relaxation is used to achieve a fast convergence rate [19]. Parallel computing is implemented to save wall clock simulation time [20]. The RANS solver is validated for CFJ static airfoil simulation [6, 9, 21, 22].

3.2 Boundary Conditions

The 3rd order accuracy no slip condition is enforced on the solid surface with the wall treatment suggested in [23] to achieve the flux conservation on the wall. Total pressure, total temperature and flow angles are specified as the inlet boundary conditions for the upstream portion of the farfield boundary and inside the injection cavity. Constant static pressure is used for the downstream portion of the farfield boundary and inside the suction cavity.

To achieve zero net mass flux with the CFJ flow control, the mass flow exiting the injection slot must be equal to the mass flow entering the suction slot. Additionally, the jet strength must be controlled in order to reach the prescribed C_μ. The prescribed C_μ is achieved by adjusting the injection cavity total pressure. Total temperature is assumed constant during this process. The injection and suction mass flow are matched by adjusting the suction cavity static pressure. The process is iterated throughout the simulation until the specified momentum coefficient is reached and the injection and suction mass flow match within the tolerance of 1%.

3.3 Mesh

The NACA 23121 CFJ airfoil grid (Fig. 2) is constructed using the O-mesh topology in order to achieve high quality around the airfoil. The mesh uses a total of 330 points around airfoil with 210 points on the suction surface and 120 points on the pressure surface, 180 points in the direction normal to the airfoil with an additional 60 points across the jet. The total mesh size is 75,600 cells and the mesh is splitted into 14 blocks for the parallel computation. The farfield boundary is located 30 chords away from the airfoil. The first grid point is placed at $y^+ \approx 1$ to resolve the turbulent boundary layer.

The NACA 23121 baseline airfoil grid (Fig. 3) is constructed using the same strategy. The total baseline airfoil mesh size is 48,600 cells with 270 points around the airfoil and 180 points normal to the airfoil. The baseline airfoil mesh is split into 9 blocks for parallel computing.

For both baseline airfoil and CFJ airfoil, a refined O-mesh grid is constructed using 50% more points in every direction and $y^+ \approx 0.7$. The refined mesh results are within 1% of the the original mesh predictions for the lift and power consumption and withing 3% for the drag and the moment. Additionally, a C-mesh is constructed for the baseline airfoil using 150 points around the airfoil and 180 points normal to the airfoil. The total mesh size is 99,000 cells and is split into 11 blocks for parallel computing.

4 Results

The numerical simulation is performed for a Mach number of 0.15 and the Reynolds number is 6.4×10^6. In this section, the simulated baseline NACA 23121 airfoil results are presented first as the basis for comparison. A trade study is then performed for the NACA 23121 CFJ airfoil on the injection location, suction location, suction size and the resulting effects on the lift, drag, moment and energy consumption. The injection size, AoA and C_μ are fixed to 0.75% chord, 10° and 0.16 respectively to represent the typical range at which a CFJ airfoil works effectively. As the last part, an optimized airfoil is created based on the trade study in order to further study its performance with the varying AoA and C_μ.

4.1 Baseline Airfoil

The baseline airfoil Mach contours are displayed in Fig. 5 for various AoA. The flow acceleration on the suction surface reaches the peak Mach number of 0.35 at $AoA = 17°$, which is slightly greater than the stall AoA and a separation region appears at the TE of the airfoil.

The NACA 23121 experimental data are extracted from [24]. The numerically obtained forces and moment compared with experimental data are plotted in Fig. 6. The lift prediction is in very good agreement with the experimental data. The experiment has a sharper stall than the CFD. The drag and moment are in good agreement with the experimental results at low AoA. At high AoA, the simulation predicts a significantly higher drag than the experiment. However the experimental value of the drag appears to be very small, especially compared to the similar experiments of T. A. Harris in [1]. The simulation predicts a large moment increases for $AoA > 12°$ because of the development of the TE recirculation. The C-mesh with twice larger grid size and different mesh topology generates almost identical results as the O-mesh. It indicates that the simulation is converged based on the mesh size and topology.

4.2 CFJ Airfoil Trade Study

As aforementioned, injection size, AoA and C_μ are fixed to 0.75% chord, 10° and 0.16 respectively for this trade study.

4.2.1 Injection Location

The injection location shown in Fig. 7 is varied from a 4% chord-wise location to a 7% chord-wise location from leading edge by increments of 1%. The injection is tangential to the local airfoil surface.

Fig. 8 shows the variation of the forces, moment and power consumption with the jet exit location. The moment remains largely unaffected over the range of injection locations tested because both the jet reactionary forces and leverage distances have only small variations. Based on the injection jet force described by Eqs.(3) and (4), if the injection slope is negative with respect to the horizontal, the jet will have a positive lift contribution. If the slope is positive, it will have a negative lift contribution. The slopes of the jet locations studied are all positive as shown in Fig. 7. Hence all the injection jets have a negative lift contribution. However, since the circulation is increased, the lift remains about constant as shown in Fig. 8. Fig. 8 also shows that a more downstream injection location increases the thrust because the injection slope is closer to zero and the injection momentum is more in the stream-wise direction. However the power consumption is slightly increased when the injection slot is moved downstream due to the higher local main flow pressure, which requires a higher pump total pressure to overcome. Overall the C_D reduction is balanced by the increase of power consumption and the corrected aerodynamic efficiency has little variation. The last plot in Fig. 8 is the aerodynamic L/D, which is in the range from nearly 200 to 400. This is a typical behavior for CFJ airfoils since the drag is reduced substantially, or even negative (thrust generation).

However, when the $(L/D)_c$ is considered with the energy consumption, the value is dropped to the range of 20. The L/D should be used for aircraft design payload and engine selection. The $(L/D)_c$ should be used for aircraft energy consumption. The 6% chord-wise injection location is used for the rest of the trade study because of its slightly higher efficiency.

4.2.2 Suction Slot Size

The suction slot size shown in Fig. 9 is varied from 1.05% chord to 1.5% chord by increments of 0.15%. As the suction slot size is increased, the suction pressure increases as well to keep the suction mass flow constant. Both the increase of size and pressure increase the overall pressure forces on the suction slot and reduces the overall nose-down moment. Those forces are balanced by the changes in pressure repartition over the airfoil and the lift and drag are slightly decrease. The power consumption increases when the suction size decreases because the smaller suction area requires a lower pressure to suck-in the same mass flow. The suction size 1.35% chord, 80% larger than the injection slot size, is used for the rest of the trade study because of its higher efficiency.

4.2.3 Suction Location

The suction location shown in Fig. 11 is varied from 70% chord-wise location to 40% by increment of 10%. A more downstream suction location increases the lift and decreases the drag as shown in Fig. 12 since a longer jet has more space to mix and energize the flow and increases the circulation. A longer jet however comes at the price of a higher energy consumption and the corrected aerodynamic efficiency is decreased. The suction-induced positive moment is increased when the suction is located more upstream due to the suction slot reactionary force and a longer moment arm. Consequently, the suction location of 40% has the best corrected aerodynamic efficiency and the smallest moment value. We select the 40% suction location configuration for the final CFJ airfoil even though this choice is arguable because of the reduced lift and increased drag when compared to the 70% suction location.

4.2.4 Airfoil Thickness

The CFJ airfoil thickness is varied from 12% to 21% as shown in Fig. 13. All airfoils are generated with an injection located at 6% chord, except the 12% thickness airfoil which is generated with both 6% and 4% chord injection locations. The corresponding forces, moment and power consumption are displayed in Fig. 14. The lift is increased with the airfoil thickness because the circulation is increased. The drag is decreased for the thinner airfoils because the more horizontal jet generates more thrust. The drag is increased for an injection located at 4% chord since the injection has a smaller streamwise component than for 6% chord location. The nose-down moment is reduced with thinner airfoils because of the reduced moment arm distance from the jet to quarter chord. Surprisingly moving the jet forward to 4% for the 12% thickness airfoil slightly decrease the nose-down moment while previous study showed no dependency of the moment on the jet exit location. This might be due to the important increase of circulation at the LE generated by the 4% jet location on the thin airfoil. If the jet exit location is kept at 6%, the energy consumption of thinner airfoil is significantly increased which reduces their efficiency. This is because for thinner airfoils the lowest pressure point is shifted closer to the LE making the injection location of 6% not optimal. This is confirmed by the very good efficiency of the 12% thickness with the injection located at 4% chord that matches the efficiency of the 21% thickness airfoil with jet located at 6%. The thickness ratio of 21% is selected for the final CFJ airfoil geometry.

4.2.5 Reynolds Number

The Reynolds number is varied from 0.8×10^6 to 12.8×10^6 for the geometry displayed in Fig. 17 and the results are shown Fig. 15. Viscous forces are more important at low Reynolds number. As a result, the drag and power consumption increase and the efficiency decreases when the Reynolds number is decreased. The lift which is mostly due to pressure forces is little affected by the Reynolds number changes. The airfoil performance becomes insensitive to Reynolds number when it is greater than 6×10^6.

4.3 Final CFJ Airfoil from Trade Study

In the trade studies above, the corrected aerodynamic efficiency was increased from 19.4 to 21.2 as seen in Fig. 16 and the final CFJ airfoil geometry is displayed on Fig. 17. This section study the final CFJ airfoil aerodynamic performance with varying AoA and C_μ. The airfoil features a thickness of 21% chord, an injection size of 0.75% chord located at 6% chord and a suction size of 1.35% chord located at 40% chord.

Fig. 18 shows the final airfoil Mach contours variation with the AoA at $C_\mu = 0.16$. The main flow peak Mach number reaches about 0.55 downstream the LE on suction surface, a large increase compared with the peak Mach number of the baseline airfoil without flow control. The injection mach number increases slightly with the AoA and reached 0.55 at $AoA = 30.0^\circ$, a 3% increase compared to $AoA = 0.0^\circ$. Downstream the injection, the jet velocity decreases faster when the AoA increases because of the increased adverse pressure gradient between the injection and the suction slot. For $AoA < 30.0^\circ$, the jet maintains a fairly high momentum going into the suction slot and makes the pumping energy consumption low. However at $AoA = 30.0^\circ$ the jet loses much of its momentum to the severe adverse pressure gradient and the pumping power is increased. At $AoA > 30.0^\circ$ the airfoil, can not sustain the large adverse pressure gradient and a recirculation region appears at the TE.

The AoA and C_μ of the final CFJ airfoil is varied and the corresponding forces, moment and power consumption are displayed in Fig. 19. The results are compared with the simulated baseline forces and moment. At high AoA, unsteady simulations are conducted to capture the boundary-layer separation and turbulent mixing. The lift is greatly enhanced by the use of CFJ with $C_Lmax = 2.91$ at $AoA = 32.5^\circ$ and $C_\mu = 0.16$, $C_Lmax = 2.52$ at $AoA = 25.0^\circ$ and $C_\mu = 0.12$ and $C_Lmax = 2.01$ at $AoA = 20.0^\circ$ and $C_\mu = 0.08$, a significant improvement compared with the baseline airfoil that reaches a maximum C_L of 1.50 at $AoA \approx 16^\circ$. The CFJ airfoil drag is significantly reduced for all C_μ with a minimum value approaching zero at $AoA = 0^\circ$ and $C_\mu = 0.16$. The moment coefficient is fairly flat until $AoA \approx 15^\circ$ and rapidly increases after. This moment increase is due in part to a flow recirculation developing at the airfoil TE at high AoA. The power coefficient is decreased with the increasing AoA before the recirculation occurs. A similar power coefficient behavior was observed during the wind tunnel testing in [25] and the simulations in [9]. The mechanism is that when the AoA increases, the LE suction is stronger and the pressure of the main flow surrounding the injection slot is lower, hence reducing the pumping power to generate the jet. When the AoA is too high however, the jet total pressure losses are increased due to the large adverse pressure gradient and in turn the pumping power is increased. At $C_\mu = 0.16$, the efficiency and power consumption of the CFJ airfoil reaches $E = 36.8$ and $Pc = 0.036$ at $AoA = 22.5^\circ$. The efficiency and power consumption are considerably improved for the lower C_μ and reach $E = 43.3$ and $Pc = 0.019$ at $AoA = 20.0^\circ$ and $C_\mu = 0.12$, and $E = 51.5$ and $Pc = 0.009$ at $AoA = 15.0^\circ$ and $C_\mu = 0.08$. The baseline airfoil is efficient at low C_L but is surpassed by the CFJ airfoil both in term of maximum lift and efficiency at high C_L. The baseline airfoil achieves its maximum efficiency at $C_L = 0.8$, whereas the CFJ airfoil reaches it at $C_L = 2.62$ for $C_\mu = 0.16$. The pure aerodynamic efficiency is tremendously improved for the CFJ airfoil and reaches $L/D = 130$ at $C_\mu = 0.16$, an increase of more than 100% compared to the baseline airfoil.

The CFJ airfoil provides a tremendous increase of maximum C_L with a high corrected aerodynamic efficiency and low nose-down moment, largely outperforming the slotted flap airfoil performance shown in [1].

5 Conclusion

The trade study indicates that the jet location and AoA are influential parameters for the energy consumption and aerodynamic efficiency. To improve the aerodynamic efficiency, the jet injection location should be at or slightly downstream the lowest pressure point on the suction surface because a low jet exit pressure reduces the pumping power. The pitch-down moment and energy consumption are reduced when the suction is located more upstream. The lift and drag are improved when the suction is located more downstream. The energy consumption is reduced with increasing AoA until the flow is separated at $AoA > 27.5°$. CFJ airfoils provide a tremendous increase of maximum C_L with a high corrected aerodynamic efficiency and low nose-down moment, largely outperforming the slotted flap airfoil performance shown in [1]. The applications for CFJ airfoils are numerous. Take-off, climbing and landing phases are particularly suitable conditions because the low free stream Mach number reduces the power consumption (Eq. (8)). Take-off and landing distances would be tremendously reduced by the use of CFJ and the climbing slope greatly increased, contributing to a reduction of the perceived noise on the ground. On the contrary, the use of flaps and slats during the climbing phase is limited because of the large amount of drag and moment that they generate. CFJ airfoils also show great potential to enhance aircraft maneuverability, especially during a sustained high G turn that requires both a tremendous maximum C_L and a relatively low drag. Another radical use of CFJ would be the implementation of CFJ to enhance the payload by increasing the cruise C_L while keeping the drag low. Finally CFJ could be used to assist the main propulsion system because of the thrust that the jet provides. More CFJ airfoils are studied in the second part of this article [26] that focuses on lowering the drag and the nose-down moment.

References

[1] T. A. Harris and R. S. Swanson, "Wind-tunnel tests of an NACA 23021 airfoil equipped with a slotted extensible and plain extensible flap ." Technical Note No. 782, NACA, November 1940.

[2] G.-C. Zha and D. C. Paxton, "A Novel Flow Control Method for Airfoil Performance Enhancement Using Co-Flow Jet." *Applications of Circulation Control Technologies*, Chapter 10, p. 293-314, Vol. 214, Progress in Astronautics and Aeronautics, AIAA Book Series, Editors: Joslin, R. D. and Jones, G.S., 2006.

[3] G.-C. Zha, W. Gao, and C. Paxton, "Jet Effects on Co-Flow Jet Airfoil Performance," *AIAA Journal, No. 6,*, vol. 45, pp. 1222–1231, 2007.

[4] G.-C. Zha, C. Paxton, A. Conley, A. Wells, and B. Carroll, "Effect of Injection Slot Size on High Performance Co-Flow Jet Airfoil," *AIAA Journal of Aircraft*, vol. 43, 2006.

[5] G.-C. Zha, B. Carroll, C. Paxton, A. Conley, and A. Wells, "High Performance Airfoil with Co-Flow Jet Flow Control," *AIAA Journal*, vol. 45, 2007.

[6] Wang, B.-Y. and Haddoukessouni, B. and Levy, J. and Zha, G.-C., "Numerical Investigations of Injection Slot Size Effect on the Performance of Co-Flow Jet Airfoil," *Journal of Aircraft*, vol. 45, No. 6, pp. 2084–2091, 2008,.

[7] B. P. E. Dano, D. Kirk, and G.-C. Zha, "Experimental Investigation of Jet Mixing Mechanism of Co- Flow Jet Airfoil." AIAA-2010-4421, 5th AIAA Flow Control Conference, Chicago, IL, 28 Jun - 1 Jul 2010.

[8] B. P. E. Dano, G.-C. Zha, and M. Castillo, "Experimental Study of Co-Flow Jet Airfoil Performance Enhancement Using Micro Discreet Jets." AIAA Paper 2011-0941, 49th AIAA Aerospace Sciences Meeting, Orlando, FL, 4-7 January 2011.

[9] A. Lefebvre, B. Dano, M. D. Fronzo, W. B. Bartow, and G-C. Zha, "Performance of a Co-Flow Jet Airfoil with Variation of Mach Number," *AIAA paper 2013-490*, Jan 2013.

[10] A. Lefebvre, G-C. Zha, "Numerical Simulation of Pitching Airfoil Performance Enhancement Using Co-Flow Jet Flow Control," *AIAA paper 2013-2517*, June 2013.

[11] Wang, B.-Y. and Haddoukessouni, B. and Levy, J. and Zha, G.-C., "Numerical Investigations of Injection Slot Size Effect on the Performance of Co-Flow Jet Airfoil ," *AIAA Journal of Aircraft*, vol. 45, pp. 2084–2091, 2008.

[12] P. Spalart and S. Allmaras, "A One-equation Turbulence Model for Aerodynamic Flows." AIAA-92-0439, 1992.

[13] Y.-Q. Shen and G.-C. Zha, "Large Eddy Simulation Using a New Set of Sixth Order Schemes for Compressible Viscous Terms ," *Journal of Computational Physics*, vol. 229, pp. 8296–8312, 2010.

[14] G.-C. Zha, Y. Shen, and B. Wang, "An improved low diffusion E-CUSP upwind scheme ," *Journal of Computer & Fluids*, vol. 48, pp. 214–220, 2011.

[15] Y.-Q. Shen and G.-Z. Zha , "Generalized finite compact difference scheme for shock/complex flowfield interaction," *Journal of Computational Physics*, vol. doi:10.1016/j.jcp.2011.01.039, 2011.

[16] Shen, Y.-Q. and Zha, G.-C. and Wang, B.-Y., " Improvement of Stability and Accuracy of Implicit WENO Scheme," *AIAA Journal*, vol. 47, No. 2, pp. 331–344, 2009.

[17] Shen, Y.-Q. and Zha, G.-C. and Chen, X.-Y., " High Order Conservative Differencing for Viscous Terms and the Application to Vortex-Induced Vibration Flows," *Journal of Computational Physics*, vol. 228(2), pp. 8283–8300, 2009.

[18] Shen, Y.-Q. and Zha, G.-C. , " Improvement of the WENO Scheme Smoothness Estimator," *International Journal for Numerical Methods in Fluids*, vol. DOI:10.1002/fld.2186, 2009.

[19] G.-C. Zha and E. Bilgen, "Numerical Study of Three-Dimensional Transonic Flows Using Unfactored Upwind-Relaxation Sweeping Algorithm," *Journal of Computational Physics*, vol. 125, pp. 425–433, 1996.

[20] B.-Y. Wang and G.-C. Zha, "A General Sub-Domain Boundary Mapping Procedure For Structured Grid CFD Parallel Computation," *AIAA Journal of Aerospace Computing, Information, and Communication*, vol. 5, No.11, pp. 2084–2091, 2008.

[21] Wang, B. Y and Zha, G.-C. , "Detached-Eddy Simulation of a Co-Flow Jet Airfoil at High Angle of Attack." AIAA Journal of Aircraft, Vol. 48, No. 5, 2011.

[22] Im, H. , Zha, G.-C., and Dano, B. P. E., "Large Eddy Simulation of Coflow Jet Airfoil at High Angle of Attack." Journal of Fluids Engineering, Vol. 136 / 021101-1, Feb. 2014.

[23] Y.-Q. Shen, G.-C. Zha, and B.-Y. Wang, "Improvement of Stability and Accuracy of Implicit WENO Scheme ," *AIAA Journal*, vol. 47, pp. 331–344, 2009.

[24] Ira H. Abbott, A. E. von Doenhoff, *Theory of Wing Sections*. Courier Dover Publications, 2012.

[25] B. Dano, A. Lefebvre and G-C. Zha, "Flow mixing mechanism of a discrete co-flow jet airfoil," *AIAA paper 3097-113*, 2011.

[26] A. Lefebvre, G-C. Zha, "Cow-Flow Jet Airfoil Trade Study Part II : Moment and Drag," *Proceedings of the AIAA Flow Control Conference*, June 2014.

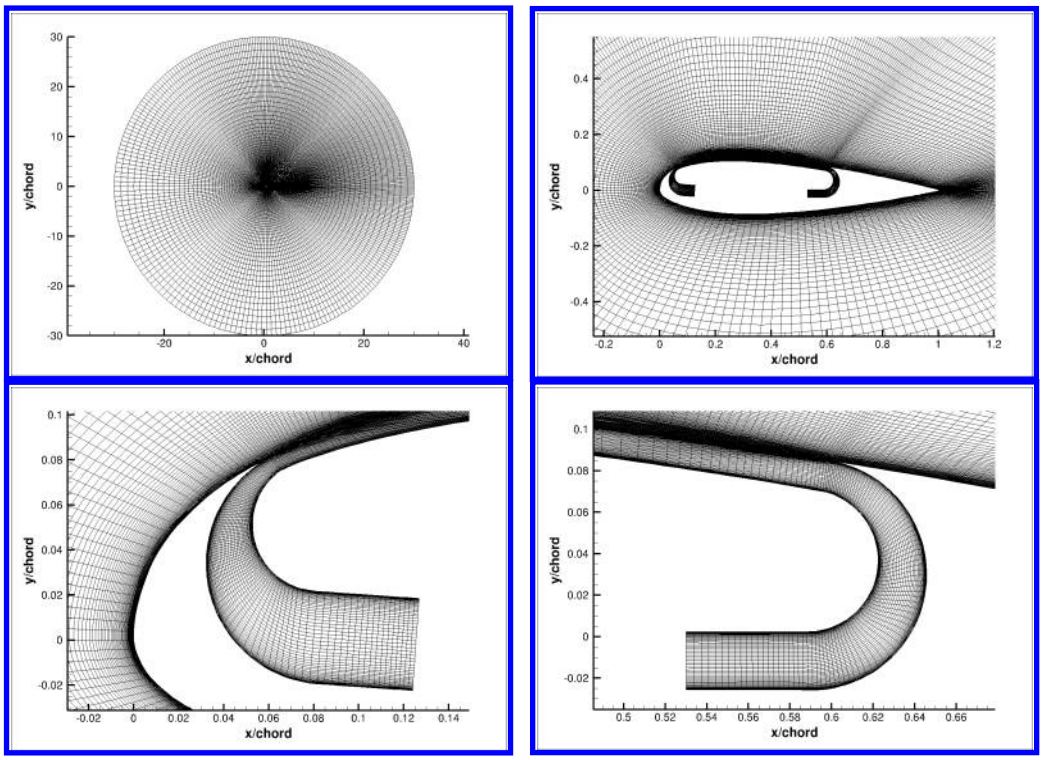

Figure 2: NACA 23121 CFJ airfoil O-mesh topology.

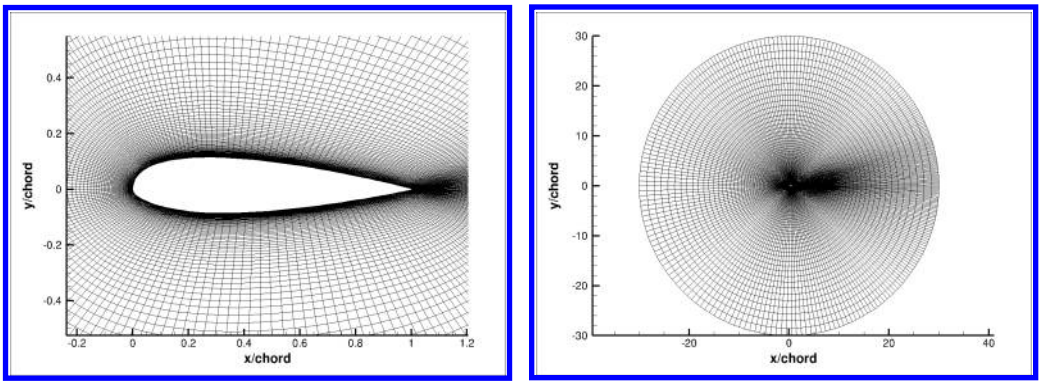

Figure 3: NACA 23121 baseline airfoil O-mesh topology.

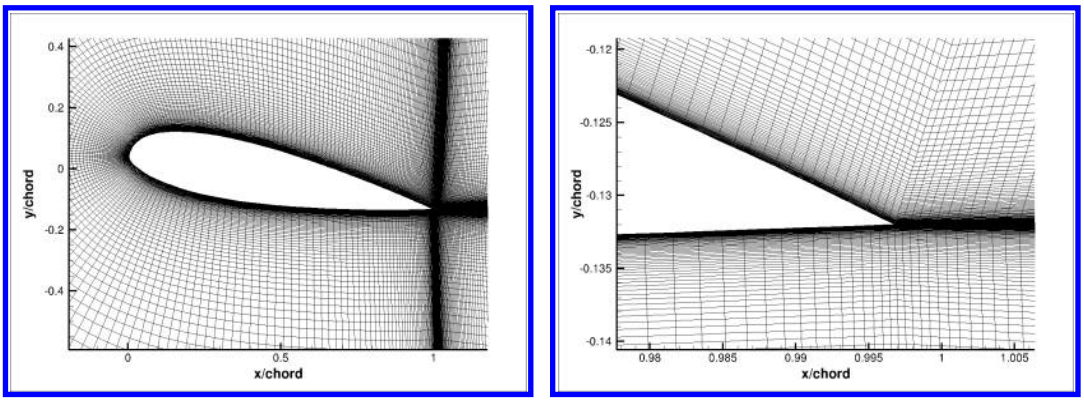

Figure 4: NACA 23121 baseline airfoil C-mesh topology.

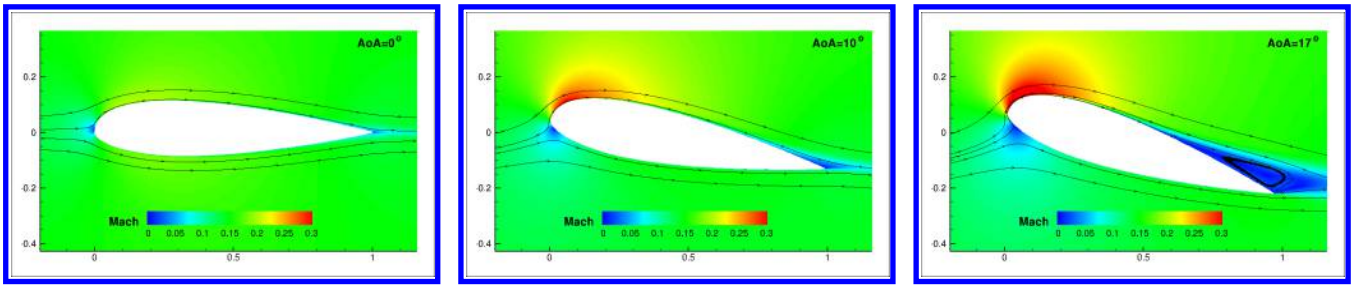

Figure 5: NACA 23121 baseline Mach contours at different AoA.

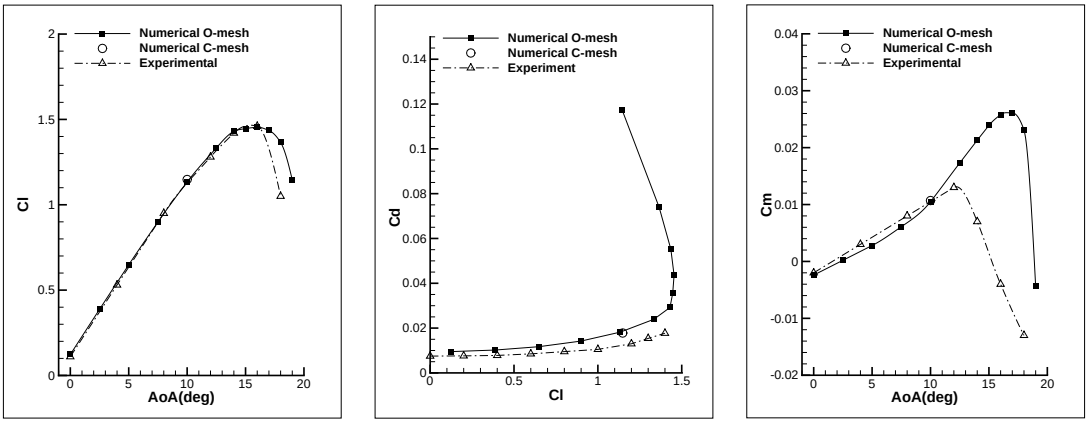

Figure 6: Numerically obtained forces and moment compared with experimental data for the NACA 23121 geometry.

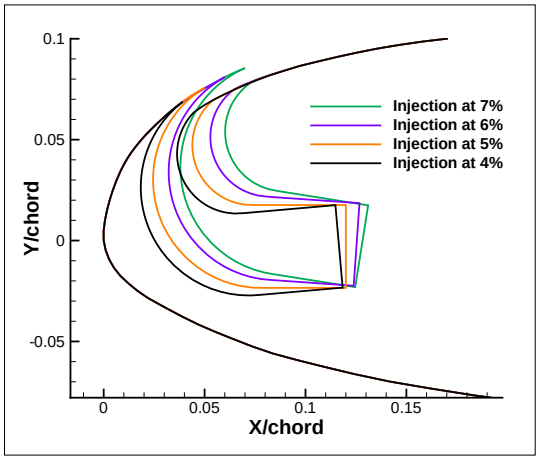

Figure 7: Geometries with variable jet exit location.

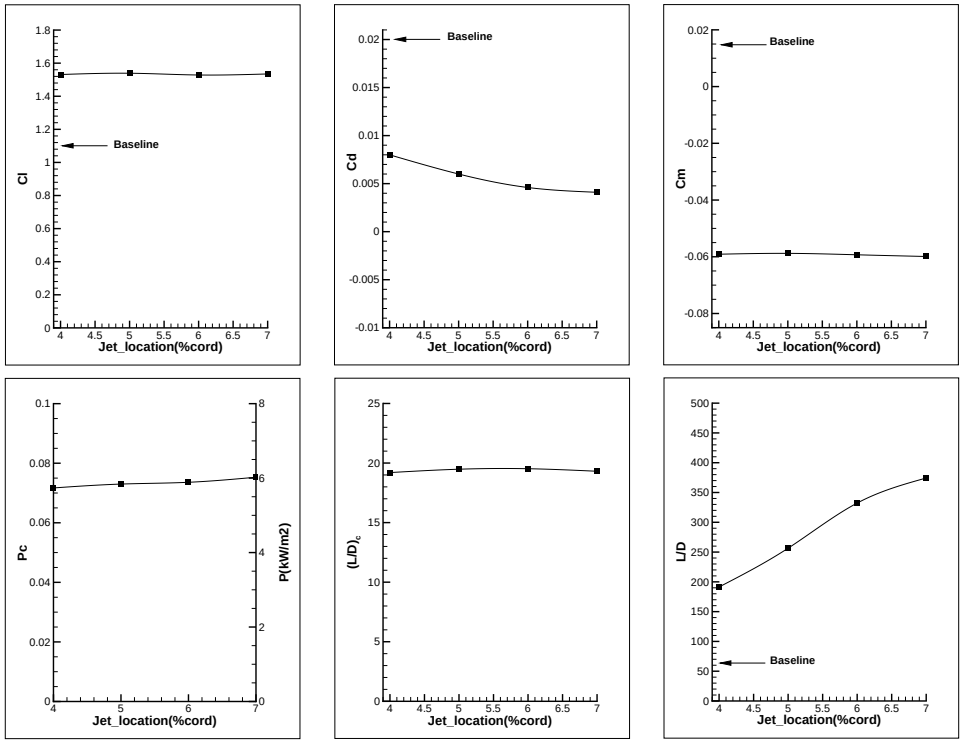

Figure 8: Variation of forces, moment and power consumption with the jet exit location at $AoA = 10^{\circ}$ and $C_{\mu} = 0.16$.

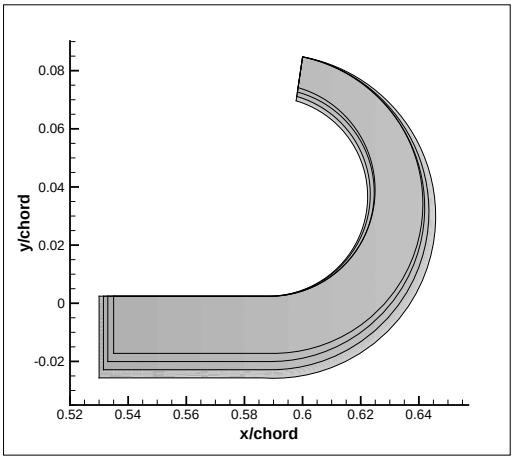

Figure 9: Overlay of the suction geometries.

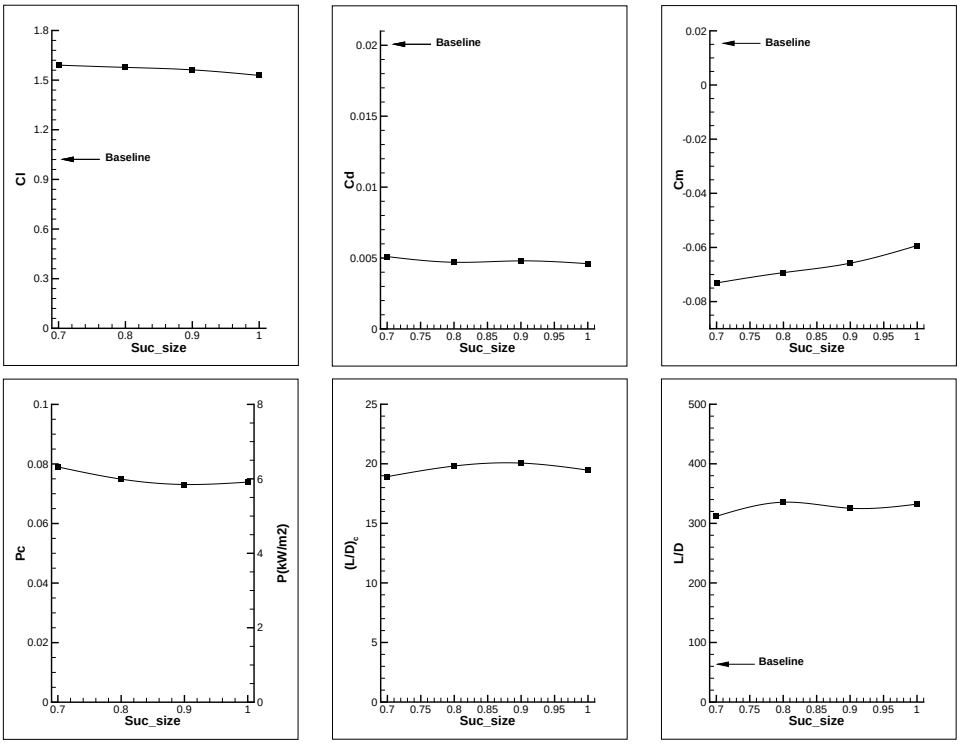

Figure 10: Variation of forces, moment and power consumption with suction size at $AoA = 10^{\circ}$ and $C_{\mu} = 0.16$. The horizontal axis represents the ratio of the current suction size to the original suction size which is 1.5%chord.

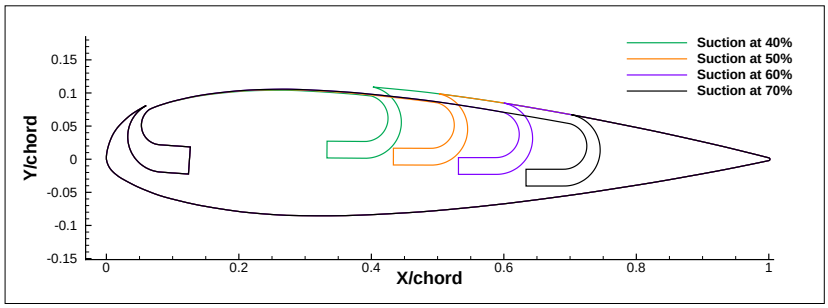

Figure 11: Geometries overlapped for the different suction location.

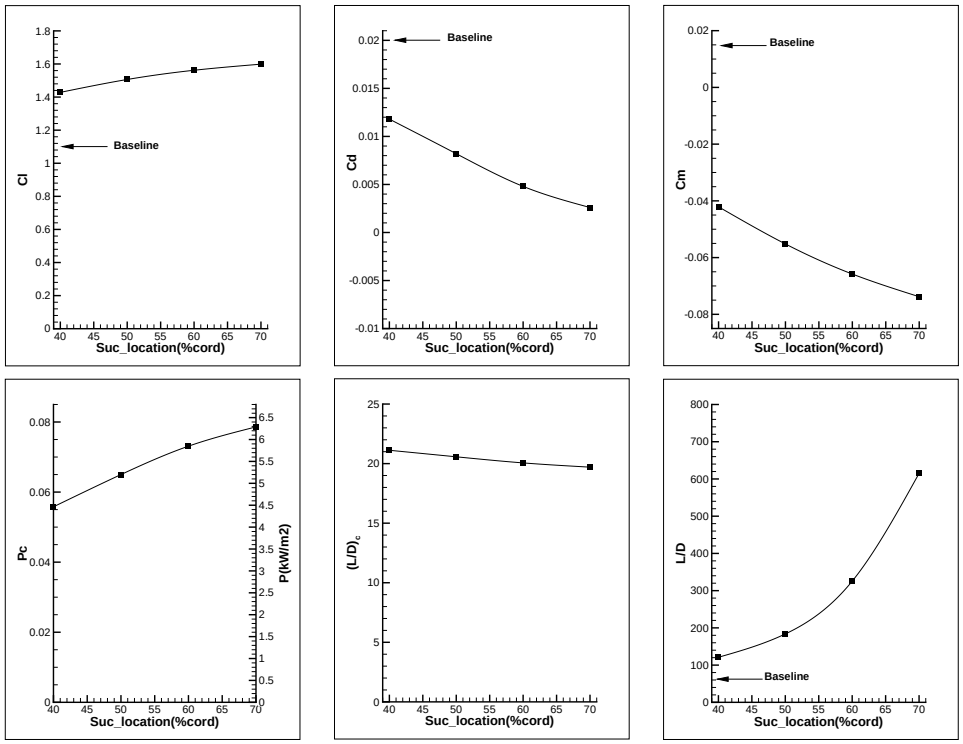

Figure 12: Variation of forces, moment and power consumption with suction location at $AoA = 10^{\circ}$ and $C_{\mu} = 0.16$.

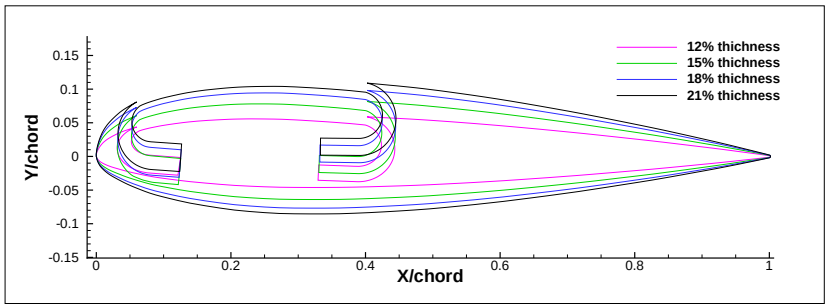

Figure 13: Thickness study overlapped geometries. In addition an airfoil with a 4% jet exit location is generated for the 12% thickness airfoil.

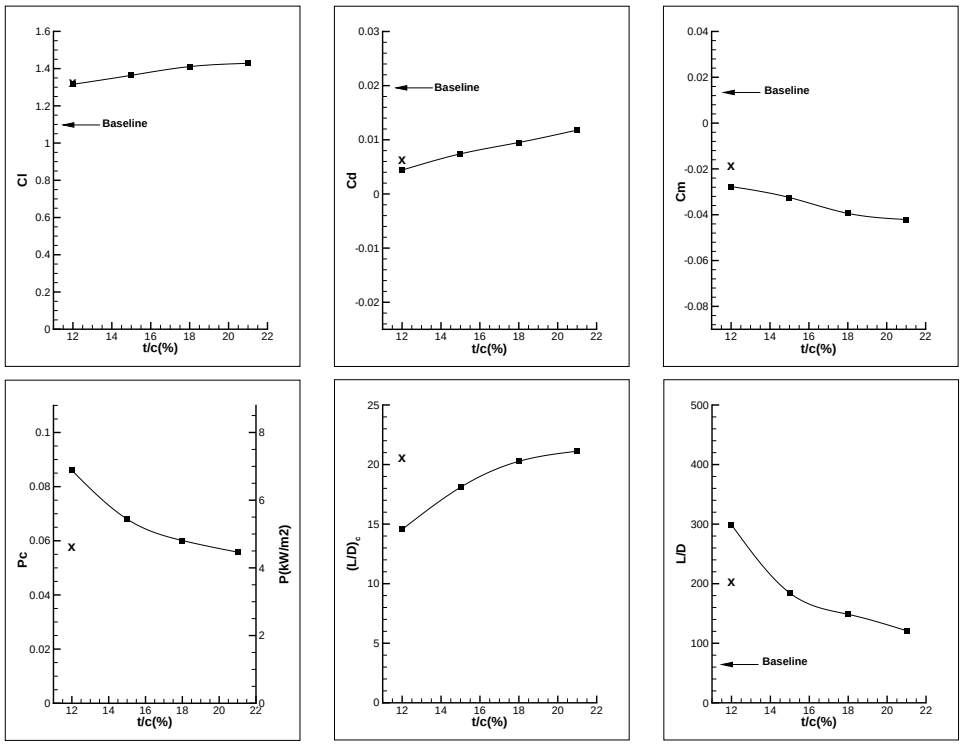

Figure 14: Variation of forces, moment and power consumption with airfoil thickness at $AoA = 10^{\circ}$ and $C_{\mu} = 0.16$. The black squares data stand for the 6% jet exit location while the crosses data stands for the 4% jet exit location.

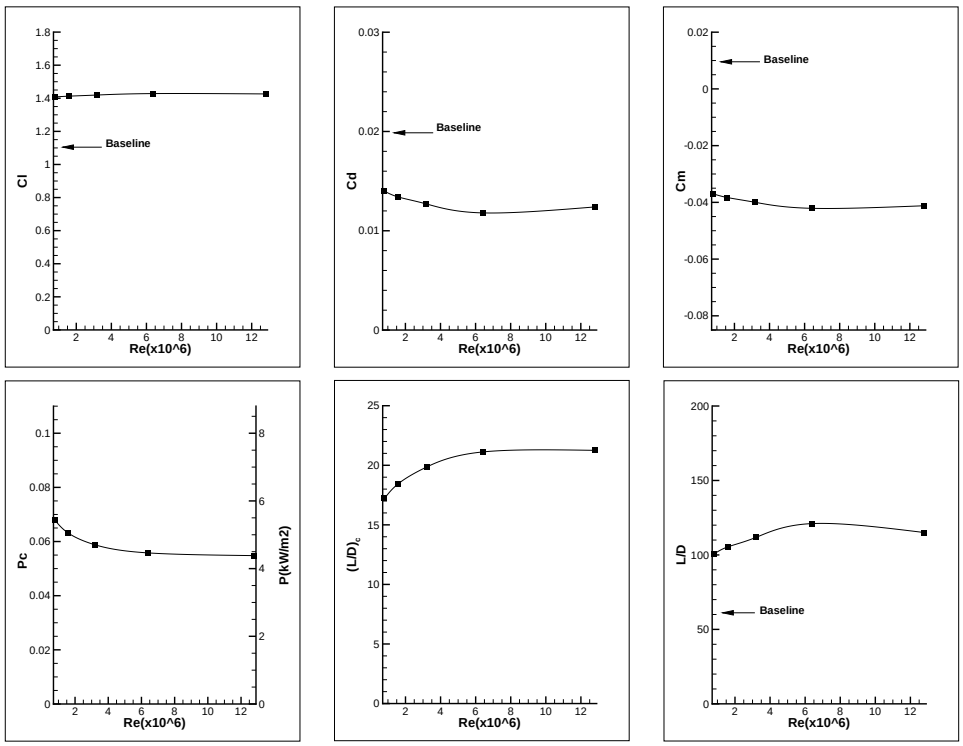

Figure 15: Variation of forces, moment and power consumption with Reynolds number at $AoA = 10^{\circ}$ and $C_{\mu} = 0.16$.

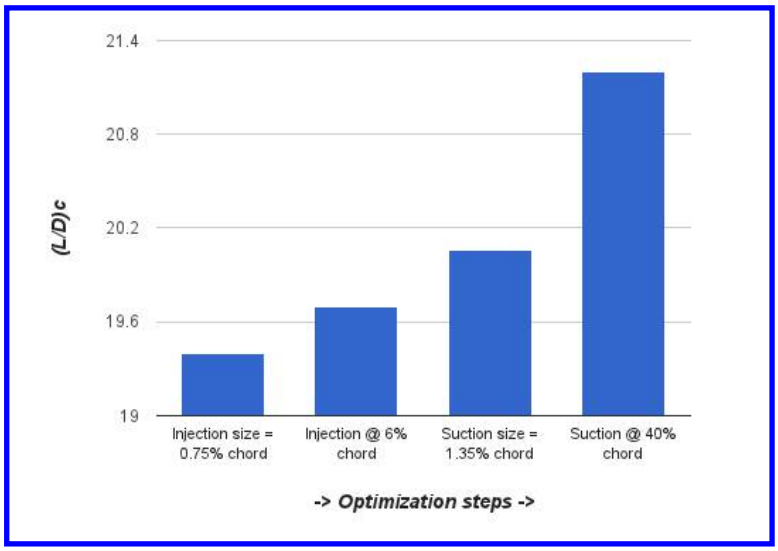

Figure 16: Corrected aerodynamic efficiency gain during CFJ trade study at $AoA = 10^{\circ}$ and $C_{\mu} = 0.16$.

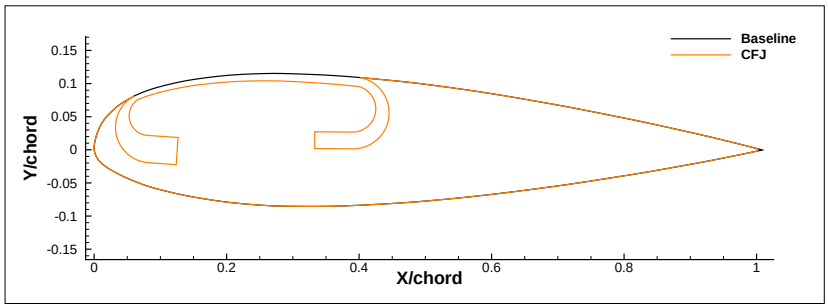

Figure 17: Final airfoil geometry accordingly to the trade study on the injection and suction size and location.

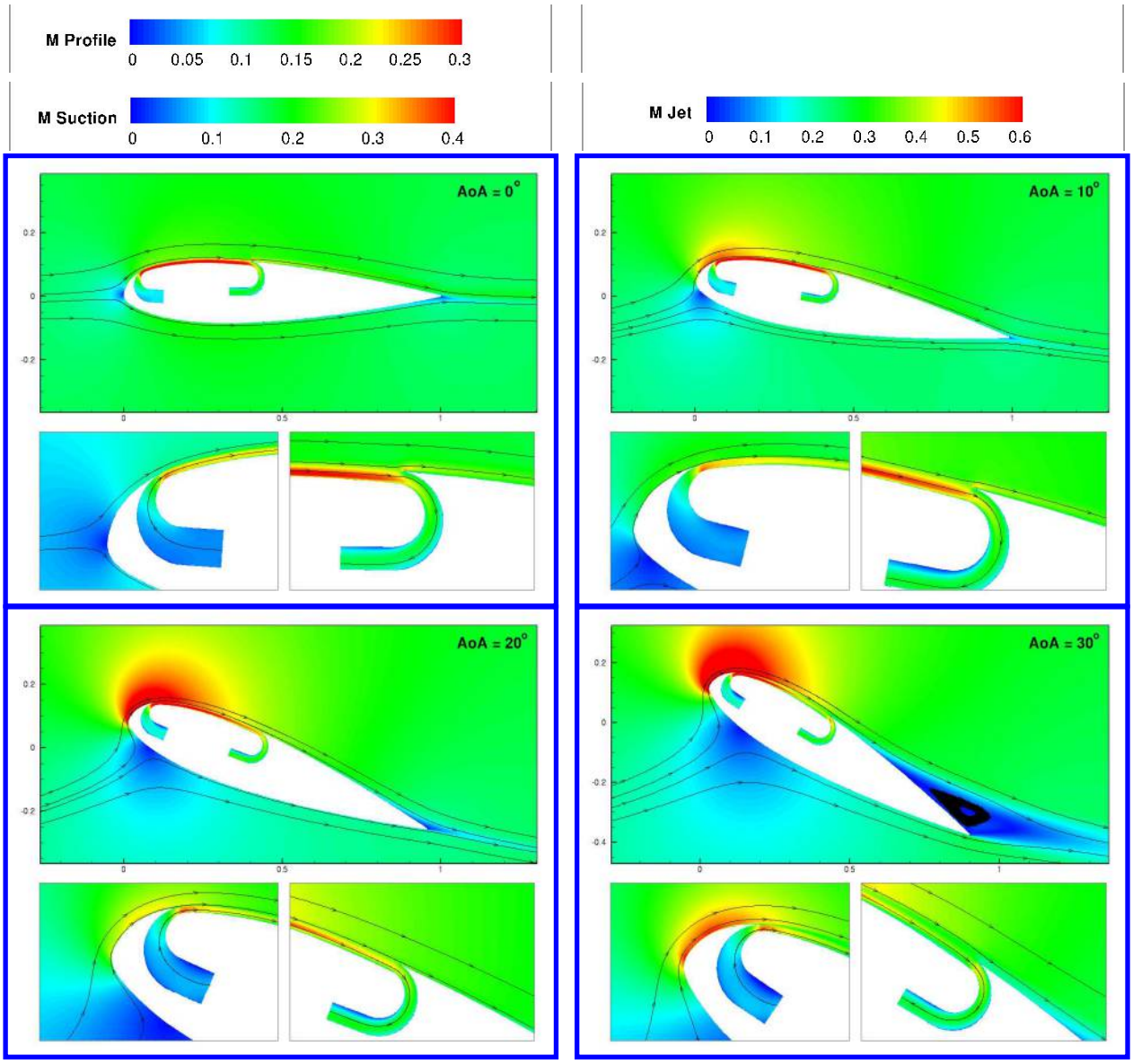

Figure 18: Final airfoil Mach contours variation with AoA at $C_\mu = 0.16$. Images include zoom in pictures of suction and injection areas.

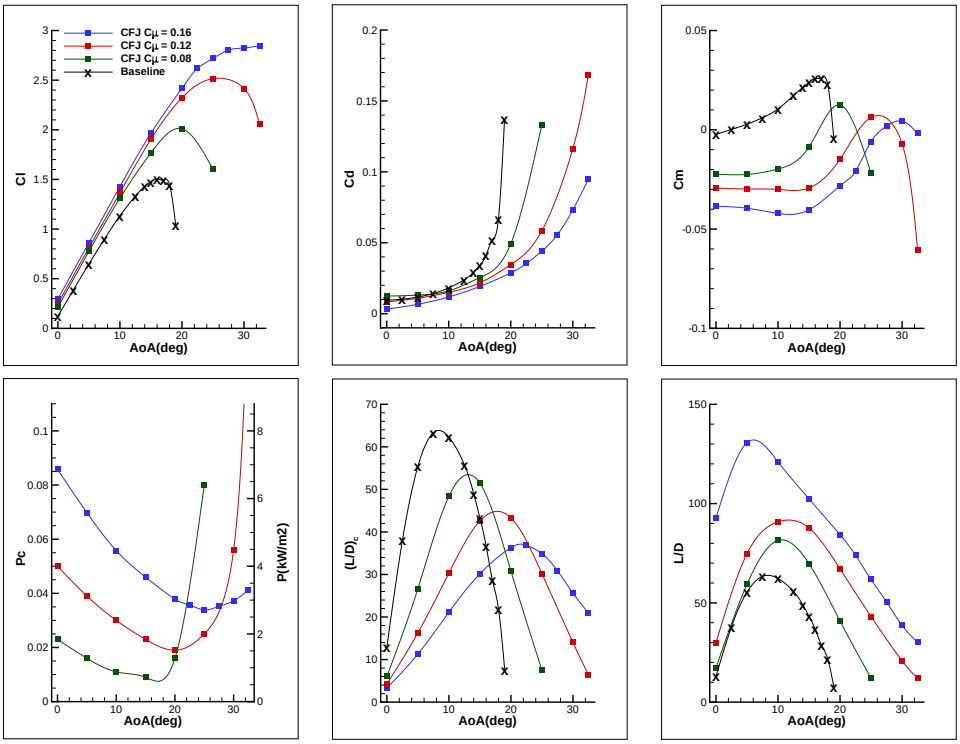

Figure 19: Final airfoil variation of forces, moment and power consumption with AoA for various C_μ.